An Optical-based Aggregate Approach to Measuring Condensation Heat Transfer

Kimberly A. Stevens, Julie Crockett, Daniel R. Maynes, Brian D. Iverson
Department of Mechanical Engineering
Brigham Young University
Provo, UT USA

1 Introduction

Condensation heat transfer is significant in many applications such as such as desalination, energy conversion [1], atmospheric water harvesting [2, 3], electronics cooling, and other high heat flux applications [4]. However, condensate on the surface adds a thermal resistance that limits condensation rates. The rate of condensation heat transfer is inversely proportional to the diameter of the condensate drops [5]. In industrial condensing systems, the resistance is minimized by removing the condensate via gravity or a vapor shear, but the minimum size of droplet removal is typically on the order of the capillary length of the condensate, about 2.7 mm for water.

Properly designed superhydrophobic surfaces have been shown to promote the removal of condensate at sizes significantly below the capillary length due to the low contact angle hysteresis and coalescence-induced jumping of condensate drops. With the removal of condensate drops due to coalescence-induced jumping, the maximum droplet diameter can be reduced by 1 to 3 orders of magnitude [6, 7]. The potential for superhydrophobic surfaces to significantly impact condensation heat transfer has promoted a great deal of exploratory research regarding the fundamental behavior of condensing droplets on superhydrophobic surfaces. Several works have quantified metrics which indirectly indicate the relative rate of heat transfer on a surface, such as maximum droplet diameter, drop size distribution, and individual droplet growth rates. Additionally, several models for condensation on superhydrophobic surfaces have been developed [8–10]. However, only a few works have experimentally measured the heat transfer directly [11–13]. Their primary focus was on the heat transfer enhancement that could be achieved with superhydrophbic surfaces relative to traditional surfaces, but in each case only a single type of superhydrophobic surface was tested, and no comparison between different types of superhydrophobic surfaces has been performed. The objective of this work is to develop a method for performing full-field optical-based heat flux measurements in order to more directly measure the rate of heat transfer, allowing more direct comparison of heat transfer performance under varying condensing conditions and surface designs.

2 Background
2.1 Superhydrophobic Surfaces

A superhydrophobic surface has a solid-liquid contact angle (CA) greater than $150°$ [14], as shown in Figure 1, and contact angle hysteresis less than $10°$. Contact angle hysteresis is the difference between the advancing and receding contact angles, and is an indicator of droplet mobility. Advancing and receding angles are the maximum and minimum contact angles a drop ever experiences, such as when volume is being slowly added or removed from a static droplet. Another metric for describing droplet mobility is the sliding angle, or the minimum angle at which a surface can be inclined before a drop placed on the surface will slide off.

Superhydrophobic surfaces are created by adding micro- or nano-structured features and then changing the surface chemistry to be hydrophobic. This is commonly accomplished by adding a hydrophobic coating. A wide variety of methods exist for creating a rough surface topography and coating. When a static droplet is sitting on top of a superhydrophobic surface, surface tension can prevent the liquid from penetrating into the cavities, creating a layer of air between the solid and liquid surfaces, as shown in Figure 2. In this case, the
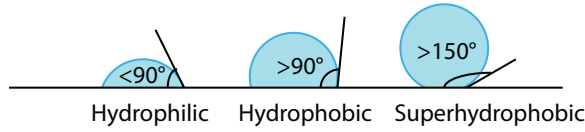
Fig. 1. The solid-liquid contact angle determines the hydrophobicity of a surface. Hydrophilic surfaces have a contact angle less than 90°, while hydrophobic surfaces have contact angles greater than 90°. Superhydrophobic surfaces have a solid-liquid contact angle of greater than 150°.

droplet is said to be in a non-wetting, or Cassie state. If the pressure in the liquid is too high, it will dominate over surface tension and liquid will enter the cavities; the surface is then said to be in a wetting, or Wenzel state. The threshold for the pressure required for the liquid to wet a superhydrophobic surface is traditionally given by the Laplace pressure, given by the Young-Laplace Equation:

$$\Delta P = P_{water} - P_{air} = \gamma(\frac{1}{R_1} + \frac{1}{R_2}) \qquad (1)$$

where γ is the surface tension, R_1 and R_2 are the surface radii of curvature. For superhydrophobic microribs, this becomes

$$\Delta P = -\frac{2\gamma cos(\theta)}{w_c} \qquad (2)$$

where θ is the contact angle for a droplet on a smooth surface of equivalent surface chemistry, and w_c is the width of the cavity between the ribs.
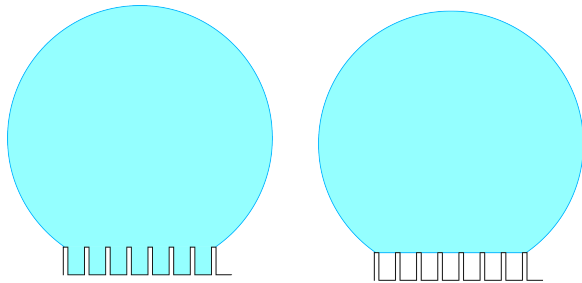

Fig. 2. When in a Wenzel sate, the liquid fills the spaces between the cavities, as shown on left. When in a non-wetting, or Cassie state, the liquid only touches the solid at a fraction of the surface, as shown on right.

2.2 Condensation on Superhydrophobic Surfaces

Initial investigations of condensation on superhydrophobic surfaces under static conditions found that the nucleation sites for condensation were evenly spread over the entire surface. As a result, a significant percentage of the initial condensate drops formed within the cavities, resulting in an irreversible wetted, or Wenzel state [15–22]. However, when Chen et al. [23] showed that drops can transition into the Cassie state when the surface has nano-scale roughness, interest in condensation on superhydrophobic surfaces was renewed. Boreyko and Chen [6] later showed that under certain conditions, condensate droplets can spontaneously jump from the surface due to the release of surface energy during coalescence. Transitioning from a wetted to non-wetted state for surfaces with nano-scale and two-tiered (micro- and nano-scale) roughness has been observed by other investigators [6, 24–28], and several models were developed that showed the potential of superhydrophobic surfaces to significantly impact the heat transfer [9, 29]. Rykaczewski [30] showed that condensate droplets do not grow with a constant contact angle, but rather grow in a stick-and-slip motion, alternating between constant contact angle and constant base area. Enright et al. [31] developed a model to predict whether a drop will be in the Cassie or Wenzel state. Though additional research needs to be done, superhydrophobic surfaces have exhibited great promise in their potential to improve heat transfer on condensing superhydrophobic surfaces.

It is well known that the majority of the heat transfer that occurs during condensation takes place in droplets smaller than 10 microns in diameter [32], and that droplets larger than 10 microns mainly grow by coalescence with other drops [30]. With the increased mobility of droplets in the Cassie state and the potential for spontaneous jumping, superhydrophobic surfaces offer the potential removal of droplets much smaller than those that can be removed by gravity alone (typically around the capillary length, about 2.7 mm for water) [5]. Miljkovic et al. [33] used the morphology model from Enright et al. [31], along with a model regarding droplet growth and coalescence, to predict the improvement in heat transfer associated with condensation on a superhydrophobic surface. Miljkovic et al. [9] demonstrated a 56% increase in heat flux for partially wetting droplets on superhydrophobic surfaces relative to a smooth hydrophobic surface. Miljkovic et al. [11] measured heat transfer on a surface which exhibited spontaneous jumping droplet behavior, which resulted in a 25% higher heat flux relative to hydrophobic surfaces at

supersaturations less than 1.12. Superhydrophobic surfaces have been shown to offer real potential for more efficient heat transfer.

3 Methods
3.1 Surface Manufacture

Surfaces with nano-scale roughness are necessary for condensate to transition to a non-wetting, or Cassie state. Droplets in the Wenzel state are highly pinned, and are not expected to perform any better than classical surfaces, and may even perform worse. A variety of methods for creating surfaces which support condensate in a Cassie state exist [34], but most techniques offer limited control over the nano-structure. For this work, a two-tiered surface was created by etching a regular microstructure consisting of a square array of pillars into a silicon wafer as described in [35] using standard photolithographic techniques and Deep Reactive-Ion Etching (DRIE). The diameter of the pillars was 6.25 microns and the center-to-center spacing between neighboring pillars was 16 microns so that the solid fraction, or area ratio between the top of the pillars and the projected surface was 12%. To create the nanostructure, the entire surface was then coated with iron, and carbon-infiltrated carbon nanotubes (CI-CNTs) were grown on the entire surface as described in [36, 37], both on top of the posts and down within the cavities. An SEM image of the surface is shown in Figure 3. The surface was functionalized by vacuum baking at 250°C for approximately 3 hours as described in [38]. The resulting surface had a static contact angle of approximately 165°and sliding angle of less than 1°. Carbon-infiltrated carbon nanotubes offer control over the nanostructure by depositing a layer of amorphous carbon on the carbon nanotubes, changing the thickness of the nanostructure [36,39,40]. Furthermore, by rendering the native carbon surface hydrophbobic, no additional chemical coating is required, creating a surface that is relatively robust compared with many of the polymer or self-assembled monolayer coatings typically used.

3.2 Condensation Setup

A condensation chamber was constructed of transparent acrylic. Inside the chamber air was bubbled through an open container of deionized water and a small fan helped accelerate evaporation, maintaining the relative humidity inside close to 70%. The superhydrophobic surface was clamped to a peltier plate with Omegatherm thermal paste at the interface to minimize
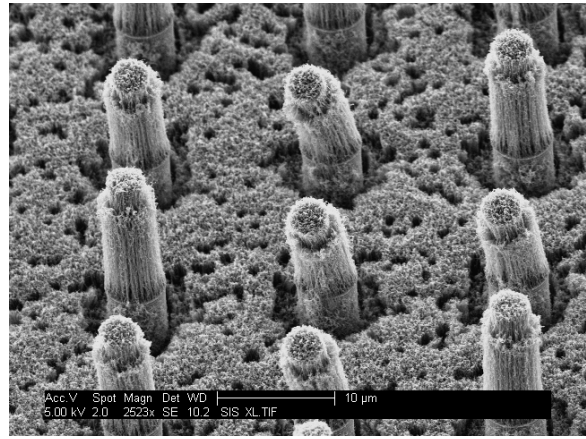

Fig. 3. An SEM image of the surface. Pillars (h=15 microns) are etched into a silicon surface, and carbon nanotubes are grown on top of the pillars. The carbon nanotubes on top of the pillars extend above the carbon nanotubes which nearly fills the cavities between the pillars.

the thermal resistance. The warm side of the peltier plate was attached to a heat sink in order to decrease the temperature achievable on the cold side. The surface was oriented vertically so that drops jumping off the surface would not return to the surface. Condensation was initiated when the condensing surface was cooled below the dew point temperature with the peltier cooler. The surface was observed using an optical microscope (Keyence VH-Z50L/W) attached to an SLR camera (Nikon D5200), and videos of the condensation were recorded at approximately 30 frames per second. The surface was illuminated using a ring light attached to the microscope lens. Once the condensation reached steady state, video was recorded.

3.3 Heat Transfer Measurement

A variety of approaches for studying condensation on superhydrophobic surfaces have been used and have provided valuable insight regarding droplet nucleation, growth, coalescence, and departure. Experiments performed in an ESEM provide detailed information regarding individual droplet nucleation and growth and have expanded to our understanding of droplet behavior. However, even with the recent significant advances in ESEM imaging, beam heating effects and temporal resolution limitations continue to be a challenge, besides the fact that the ESEM does not allow direct macroscopic heat transfer measurements. Thermocouple measurements can provide an overall heat flux, but are difficult to implement with high levels of accuracy. Optical microscopes lack the magnification capabilities of the ESEM, but provide full-field measurements re-

garding drop spatial and size distribution. However, due to the difficulty of building a chamber capable of removing the non-condensable gases (NCG), most optical microscope measurements are performed in the presence of NCG, which dramatically inhibits condensation rates and behavior. Olceroglu et al. [12] used an optical microscope to measure the volume of condensate produced, as a measure of the latent energy transfer. They used this information to obtain a heat flux with an uncertainty of $+/-2W/m^2$, which is considerably smaller than that typically achievable using thermocouple based measurements. A similar approach was implemented in this work using a custom MATLAB code.
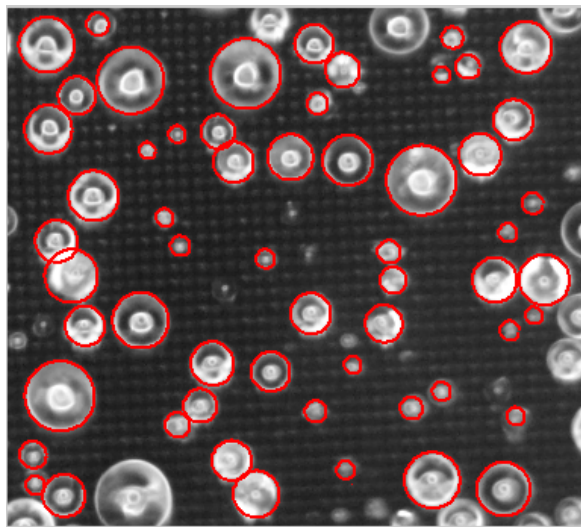

Fig. 4. A single frame of the video with all of the drops detected in that frame. The regular array of dots in the background are the tops of the silicon pillars, which are spaced 16 microns apart. Drops overlapping the edge of the field of view were not tracked.

On the first frame of the video, the location and radius of each of the drops of condensate is found using a Hough Transform. The code then tracks the growth of each droplet in the first frame through time until the drop coalesces with a neighboring drop or the video ends. On subsequent frames, additional drops that form are detected and similarly tracked through time. Figure 4 shows one frame of the video with all of the drops detected in that frame. The regular array of lighter spots in the background are the tops of the silicon pillars, which are spaced 16 microns apart. Drops overlapping the edge of the field of view were not tracked. Since the radius of the drops is larger than 10 microns, the drops should be growing in constant contact angle mode [12, 41]. Therefore, a contact angle of 165 °is used to calculate the volume (based on the detected ra-

dius) of all of the drops of condensate within the field of view of the camera. The volume is used to calculate the latent energy on the surface, as well as the latent energy of the drops which have departed the surface via coalescence-induced jumping. During steady state condensation, the latent energy of the drops on the surface remains relatively constant, and the heat flux can be estimated from the volume of drops which depart the surface. For the surface tested, the jumping did not occur for drops smaller than 10 microns. By tracking the growth of each droplet through time, metrics such as nucleation density and drop size distribution can be compared with the macroscopic heat transfer estimation. Furthermore, a wealth of information regarding individual droplet growth rates and departure diameter were collected.
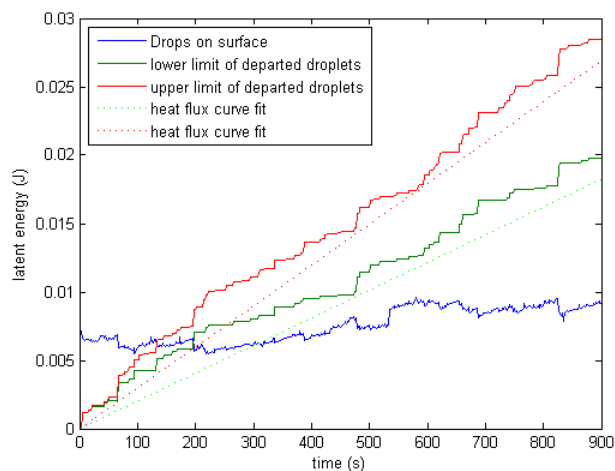

Fig. 5. Latent energy as a function of time.

4 Results and Discussion

At a magnification of 500X, the resolution of the imaging system was 0.86 microns per pixel. For an example case study, a 585 X 648 micron widow was analyzed for 900 seconds. The latent energy of the drops on the surface and the cumulative latent energy of the departed drops is shown in Figure 5. Due to the difficulty of differentiating between drops that jumped and those that simply coalesced with neighboring drops, an upper and lower bound is reported for the departed droplet latent energy. The heat transfer rate was calculated from a linear fit to the latent energy as a function of time, as indicated by the dotted line, and the average heat flux was calculated by dividing by the area of the field of view,

resulting in a heat flux of 53-79 W/m^2, corresponding to the upper and lower limits of the estimation of the departed drop energy. The low heat flux is due to the presence of non-condensable gases in the condensing chamber, and is comparable with that reported by Olceroglu et al. [12].
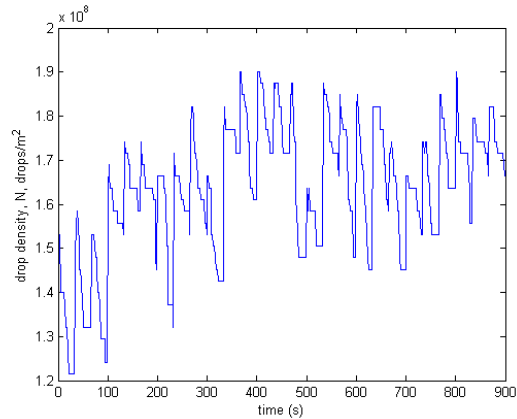

Fig. 6. Drop density as a function of time.

Fig. 7. Drop density as a function of time.

Drop density as a function of time is shown in Figure 6, and remained relatively constant, around 1.7 X 10^8 m^{-2} over the course of the video. This is slightly lower than the total reported by Olceroglu et al. [12], who reported steady state nucleation densities of approximately 1 X 10^9 to 3 X 10^9, depending on the degree of subcooling and ramp rate. However, they were measuring nucleation densities for drops with a radius as small as 1.25 microns, whereas the present study only tracked drops larger than 10 microns in radius. Olceroglu et al. [12] reported a steady state nucleation density of approximately 1 X 10^8 m^{-2} for drops 10-15 microns in radius, and approximately 8 X 10^7 m^{-2} for drops larger than 15 microns, which is comparable with the nucleation density in the present work of 1.7 X 10^8 for drops larger than 10 microns in radius.

In addition to full-field measurements, the present approach tracks the growth of individual droplets and determines what happens to the drop if it coalesces with a neighboring drop. As an example, cases where two drops coalesce and depart the surface and where two drops coalesce and do not depart are shown in Figure 7. Two drops, labeled 1 and 4, are tracked through time until they coalesce and depart from the surface. Drops 20 and 183 are tracked through time until they coalesce, when Drop 20 rapidly increases in radius. From this, detailed information regarding individual and average drop growth rates,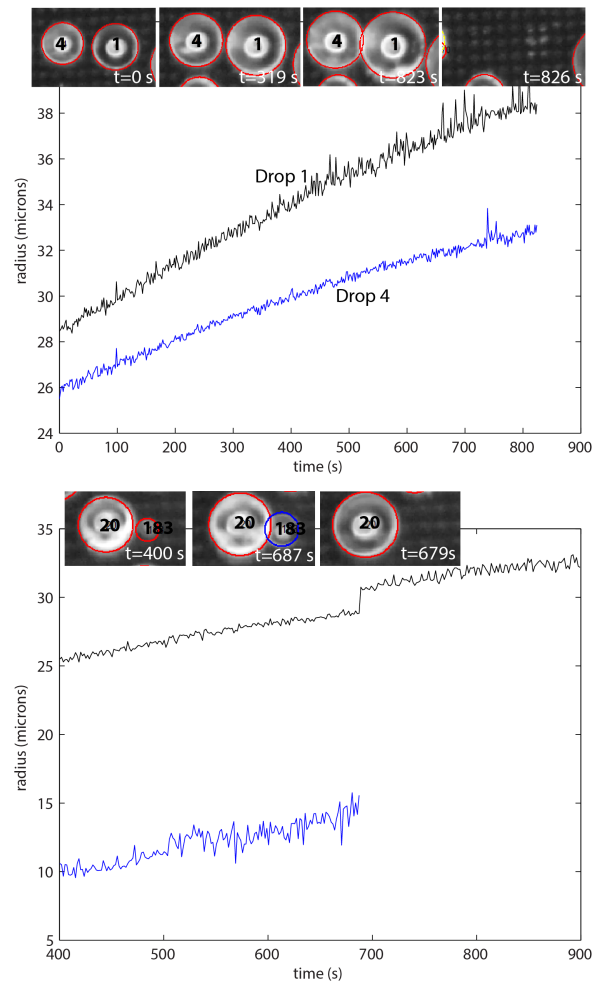 average, range, and distribution of drop size and departure radius, as well as percentage of coalescence events that result in jumping can be calculated continuously throughout time for an entire field encompassing hundreds to thousands of droplets, rather than for a few droplets or at a few discrete points in time. Such information will provide insight into the link between easily and frequently reported metrics, such the distribution of drop size and macroscopic heat transfer rates, whereas now the correlation is only speculative. It will provide data which can be used in models for condensation and provide insight into why and how various condensing conditions and surface designs affect overall heat transfer rates, as opposed to the more heuristic approach necessitated if only the overall heat flux is known.

5 Conclusion

A two-tiered surface superhydrophobic surface which offered control over both the micro- and nano-

structure was manufactured and rendered hydrophobic. A framework for providing detailed information regarding individual drop growth and behavior during condensation, as well as macroscopic full field heat transfer measurements was developed and demonstrated. Results were compared with a similar approach used by Olceroglu et al. [12]. Their work, performed in the presence of NCG, demonstrated the dependence of steady state heat flux on nucleation density, which they showed to be dependent on not only the degree of subcooling, but also the rate of subcooling during the initiation of condensation when in the presence of NCG. This important contribution further highlights the importance of performing condensation experiments in the absence of NCG. Though demonstrated on a condensing system in the presence of NCG, the present approach is compatible with condensing systems with no NCG, and future work will be performed inside a vacuum system where the NCG have been removed. Future work will also include exploration of how changing the nanostruture by controlling the thickness of the carbon nanotubes influences overall heat transfer rates.

References

[1] L. R. Glicksman and A. W. Hunt, "Numerical simulation of dropwise condensation," *International Journal of Heat and Mass Transfer*, vol. 15, no. 11, pp. 2251–2269, 1972.

[2] J. C. Love, L. A. Estroff, J. K. Kriebel, R. G. Nuzzo, and G. M. Whitesides, "Self-assembled monolayers of thiolates on metals as a form of nanotechnology," *Chemical Reviews*, vol. 105, no. 4, pp. 1103–69, 2005.

[3] H. G. Andrews, E. A. Eccles, W. C. Schofield, and J. P. Badyal, "Three-dimensional hierarchical structures for fog harvesting," *Langmuir*, vol. 27, no. 7, pp. 3798–802, 2011.

[4] R. N. Leach, F. Stevens, S. C. Langford, and J. T. Dickinson, "Dropwise condensation: experiments and simulations of nucleation and growth of water drops in a cooling system," *Langmuir*, vol. 22, no. 21, pp. 8864–72, 2006.

[5] J. W. Rose, "Dropwise condensation theory and experiment: a review," *Proceedings of the Institution of Mechanical Engineers Part a-Journal of Power and Energy*, vol. 216, no. A2, pp. 115–128, 2002.

[6] J. B. Boreyko and C.-H. Chen, "Self-propelled dropwise condensate on superhydrophobic surfaces," *Physical Review Letters*, vol. 103, no. 18, p. 184501, 2009.

[7] H. Cha, C. Xu, J. Sotelo, J. M. Chun, Y. Yokoyama, R. Enright, and N. Miljkovic, "Coalescence-induced nanodroplet jumping," *Physical Review Fluids*, vol. 1, no. 6, p. 064102, 2016.

[8] S. Kim and K. J. Kim, "Dropwise condensation modeling suitable for superhydrophobic surfaces," *Journal of Heat Transfer*, vol. 133, no. 8, pp. 081 502–081 502–8, 2011.

[9] N. Miljkovic, R. Enright, and E. N. Wang, "Effect of droplet morphology on growth dynamics and heat transfer during condensation on superhydrophobic nanostructured surfaces," *ACS Nano*, vol. 6, no. 2, pp. 1776–1785, 2012.

[10] S. Chavan, H. Cha, D. Orejon, K. Nawaz, N. Singla, Y. F. Yeung, D. Park, D. H. Kang, Y. Chang, Y. Takata, and N. Miljkovic, "Heat transfer through a condensate droplet on hydrophobic and nanostructured superhydrophobic surfaces," *Langmuir*, vol. 32, no. 31, pp. 7774–7787, 2016.

[11] N. Miljkovic, R. Enright, Y. Nam, K. Lopez, N. Dou, J. Sack, and E. N. Wang, "Jumping-droplet-enhanced condensation on scalable superhydrophobic nanostructured surfaces," *Nano Letters*, vol. 13, no. 1, pp. 179–187, 2013.

[12] E. lerolu, C.-Y. Hsieh, M. M. Rahman, K. K. S. Lau, and M. McCarthy, "Full-field dynamic characterization of superhydrophobic condensation on biotemplated nanostructured surfaces," *Langmuir*, vol. 30, no. 25, pp. 7556–7566, 2014.

[13] R. Wen, Q. Li, J. Wu, G. Wu, W. Wang, Y. Chen, X. Ma, D. Zhao, and R. Yang, "Hydrophobic copper nanowires for enhancing condensation heat transfer," *Nano Energy*, vol. 33, pp. 177–183, 2017.

[14] K.-Y. Law, "Definitions for hydrophilicity, hydrophobicity, and superhydrophobicity: Getting the basics right," *Journal of Physical Chemistry Letters*, vol. 5, p. 686688, 2014.

[15] A. Lafuma and D. Quere, "Superhydrophobic states," *Nat Mater*, vol. 2, no. 7, pp. 457–460, 2003.

[16] R. Narhe and D. Beysens, "Water condensation on a super-hydrophobic spike surface," *EPL (Europhysics Letters)*, vol. 75, no. 1, p. 98, 2006.

[17] K. A. Wier and T. J. McCarthy, "Condensation on ultrahydrophobic surfaces and its effect on droplet mobility: ultrahydrophobic surfaces are not always water repellant," *Langmuir*, vol. 22, no. 6,

pp. 2433–2436, 2006.

[18] R. D. Narhe and D. A. Beysens, "Growth dynamics of water drops on a square-pattern rough hydrophobic surface," *Langmuir*, vol. 23, no. 12, pp. 6486–6489, 2007.

[19] Y. T. Cheng and D. E. Rodak, "Is the lotus leaf superhydrophobic?" *Applied Physics Letters*, vol. 86, no. 14, 2005.

[20] Y. T. Cheng, D. E. Rodak, A. Angelopoulos, and T. Gacek, "Microscopic observations of condensation of water on lotus leaves," *Applied Physics Letters*, vol. 87, no. 19, 2005.

[21] Y. C. Jung and B. Bhushan, "Wetting behaviour during evaporation and condensation of water microdroplets on superhydrophobic patterned surfaces," *Journal of Microscopy*, vol. 229, no. 1, pp. 127–140, 2008.

[22] C. Dorrer and J. Rhe, "Condensation and wetting transitions on microstructured ultrahydrophobic surfaces," *Langmuir*, vol. 23, no. 7, pp. 3820–3824, 2007.

[23] C. H. Chen, Q. J. Cai, C. L. Tsai, C. L. Chen, G. Y. Xiong, Y. Yu, and Z. F. Ren, "Dropwise condensation on superhydrophobic surfaces with two-tier roughness," *Applied Physics Letters*, vol. 90, no. 17, 2007.

[24] C. W. Lo, C. C. Wang, and M. C. Lu, "Scale effect on dropwise condensation on superhydrophobic surfaces," *Acs Applied Materials and Interfaces*, vol. 6, no. 16, pp. 14 353–14 359, 2014.

[25] T. J. Ko, E. K. Her, B. Shin, H. Y. Kim, K. R. Lee, B. K. Hong, S. H. Kim, K. H. Oh, and M. W. Moon, "Water condensation behavior on the surface of a network of superhydrophobic carbon fibers with high-aspect-ratio nanostructures," *Carbon*, vol. 50, no. 14, pp. 5085–5092, 2012.

[26] N. Miljkovic and E. N. Wang, "Condensation heat transfer on superhydrophobic surfaces," *MRS Bulletin*, vol. 38, pp. 397–406, 2013.

[27] F. C. Wang, F. Q. Yang, and Y. P. Zhao, "Size effect on the coalescence-induced self-propelled droplet," *Applied Physics Letters*, vol. 98, no. 5, 2011.

[28] C. Dorrer and J. Rhe, "Wetting of silicon nanograss: From superhydrophilic to superhydrophobic surfaces," *Advanced Materials*, vol. 20, no. 1, pp. 159–163, 2008.

[29] C. Dietz, K. Rykaczewski, A. G. Fedorov, and Y. Joshi, "Visualization of droplet departure on a superhydrophobic surface and implications to heat transfer enhancement during dropwise con-

densation," *Applied Physics Letters*, vol. 97, no. 3, 2010.

[30] K. Rykaczewski, "Microdroplet growth mechanism during water condensation on superhydrophobic surfaces," *Langmuir*, vol. 28, no. 20, pp. 7720–7729, 2012.

[31] R. Enright, N. Miljkovic, A. Al-Obeidi, C. V. Thompson, and E. N. Wang, "Condensation on superhydrophobic surfaces: The role of local energy barriers and structure length scale," *Langmuir*, vol. 28, no. 40, pp. 14 424–14 432, 2012.

[32] C. Graham and P. Griffith, "Drop size distributions and heat-transfer in dropwise condensation," *International Journal of Heat and Mass Transfer*, vol. 16, no. 2, pp. 337–346, 1973.

[33] N. Miljkovic, R. Enright, and E. N. Wang, "Modeling and optimization of superhydrophobic condensation," *Journal of Heat Transfer*, vol. 135, no. 11, p. 111004, 2013.

[34] H. J. Cho, D. J. Preston, Y. Zhu, and E. N. Wang, "Nanoengineered materials for liquid-vapour phase-change heat transfer," *Nature Reviews Materials*, vol. 2, p. 16092, 2016.

[35] J. Prince, "The influence of superhydrophobicity on laminar jet impingement and turbulent flow in a channel with walls exhibiting riblets," Doctoral Dissertation, Brigham Young University, 2013.

[36] K. M. Marr, B. Chen, E. J. Mootz, J. Geder, M. Pruessner, B. J. Melde, R. R. Vanfleet, I. L. Medintz, B. D. Iverson, and J. C. Claussen, "High aspect ratio carbon nanotube membranes decorated with pt nanoparticle urchins for micro underwater vehicle propulsion via h2o2 decomposition," *ACS Nano*, vol. 9, no. 8, pp. 7791–7803, 2015.

[37] B. J. Brownlee, K. M. Marr, J. C. Claussen, and B. D. Iverson, "Improving sensitivity of electrochemical sensors with convective transport in free-standing, carbon nanotube structures," *Sensors and Actuators B: Chemical*, vol. 246, pp. 20–28, 2017.

[38] A. I. Aria and M. Gharib, "Dry oxidation and vacuum annealing treatments for tuning the wetting properties of carbon nanotube arrays," *Journal of Visualized Experiments : JoVE*, no. 74, p. 50378, 2013.

[39] J. Song, D. S. Jensen, D. N. Hutchison, B. Turner, T. Wood, A. Dadson, M. A. Vail, M. R. Linford, R. R. Vanfleet, and R. C. Davis, "Carbon-nanotube-templated microfabrication of porous silicon-carbon materials with application to chem-

ical separations," *Advanced Functional Materials*, vol. 21, no. 6, pp. 1132–1139, 2011.

[40] D. N. Hutchison, N. B. Morrill, Q. Aten, B. W. Turner, B. D. Jensen, L. L. Howell, R. R. Vanfleet, and R. C. Davis, "Carbon nanotubes as a framework for high-aspect-ratio mems fabrication," *Journal of Microelectromechanical Systems*, vol. 19, no. 1, pp. 75–82, 2010.

[41] K. Rykaczewski, J. H. J. Scott, and A. G. Fedorov, "Electron beam heating effects during environmental scanning electron microscopy imaging of water condensation on superhydrophobic surfaces," *Applied Physics Letters*, vol. 98, no. 9, p. 093106, 2011.